Earth and Planetary Science Letters 594 (2022) 117700

Contents lists available at ScienceDirect

Earth and Planetary Science Letters

www.elsevier.com/locate/epsl

Graphite as an electrically conductive indicator of ancient crustal-scale fluid flow within mineral systems

Benjamin S. Murphy [a,b,*], Jan Marten Huizenga [c,d,e], Paul A. Bedrosian [a]

[a] Geology, Geophysics, and Geochemistry Science Center, U.S. Geological Survey, Denver, CO 80225, USA
[b] Geomagnetism Program, U.S. Geological Survey, Golden, CO 80401, USA
[c] Faculty of Environmental Sciences and Natural Resource Management, Norwegian University of Life Sciences, P.O. Box 5003, NO-1432, Ås, Norway
[d] Economic Geology Research Centre, College of Science and Engineering, James Cook University, Townsville, Queensland 4811, Australia
[e] Department of Geology, University of Johannesburg, Auckland Park 2006, South Africa

ARTICLE INFO

Article history:
Received 16 June 2021
Received in revised form 23 June 2022
Accepted 28 June 2022
Available online xxxx
Editor: R. Dasgupta

Keywords:
mineral systems
IOA-IOCG
Olympic Dam
Southeast Missouri Iron Province
magnetotellurics
graphite

ABSTRACT

Magnetotelluric (MT) imaging results from mineral provinces in Australia and in the United States show an apparent spatial relationship between crustal-scale electrical conductivity anomalies and major magmatic-hydrothermal iron oxide-apatite/iron oxide-copper-gold (IOA-IOCG) deposits. Although these observations have driven substantial interest in the use of MT data to image ancient fluid pathways, the exact cause of these anomalies has been unclear. Here, we interpret the conductors to be the result of graphite precipitation from CO_2-rich magmatic fluids during cooling. These fluids would have exsolved from mafic magmas at mid- to lower-crustal depths; saline magmatic fluids that could drive mineralization were likely derived from related, more evolved intrusions at shallower crustal levels. In our model, the conductivity anomalies then mark zones that once were the deep roots of ancient magmatic-hydrothermal mineral systems.

1. Introduction

The mineral systems approach to resource exploration has arisen as a novel method to vector towards ore deposits. This paradigm aims to integrate disparate geoscientific data in order to formulate a model of lithospheric architecture and history that can be used to identify locations that were once conducive to deposit formation (e.g., McCuaig and Hronsky, 2014).

Magnetotelluric (MT) imaging has emerged as a key tool in the mineral systems framework, particularly due to observed spatial relationships between lithosphere-scale electrical conductivity anomalies and iron oxide-apatite (IOA) and iron oxide-copper-gold (IOCG) deposits. The premier examples of such correlations have come from the Olympic Dam region (Heinson et al., 2006, 2018) and the Cloncurry District (Jiang et al., 2019; Wang et al., 2018) in Australia as well as from the Southeast Missouri Iron Province (SMIP) in the United States (Fig. 1; e.g., McCafferty et al., 2019). At the mineral-province scale, MT imaging reveals highly conductive ($> 10^{-1}$ S/m), steeply dipping pipe- or sheet-like anomalies at mid-lower crustal depths as well as moderately conductive ($\sim 10^{-2}$ S/m) "fingers" that extend into the upper crust beneath individual deposits (e.g., Fig. 1).

Presently intracratonic, Mesoproterozoic-aged IOA-IOCG deposits in the Olympic Dam region and in the SMIP are viewed as magmatic-hydrothermal in origin. Genetic models invoke mantle-derived magmatism in an extensional setting (back-arc, orogenic collapse, or intraplate rift) to provide heat and fluids, as well as possibly metals, into the system (e.g., Day et al., 2016; McCafferty et al., 2019; Skirrow et al., 2018; see also Fig. 1C); mixing of these magmatic fluids with near-surface fluids (meteoric waters or basinal brines) in the upper crust is inferred to have driven deposit formation (e.g., Barton, 2014; Schlegel et al., 2020). In this context, the co-located electrical conductivity anomalies have loosely been interpreted as the signature of metasomatism along crustal-scale magmatic fluid pathways (e.g., Heinson et al., 2018); however, a physically rigorous explanation of these apparently associated conductors is lacking. Here, we suggest that these conductivity anomalies are specifically the result of graphite precipitation from CO_2-rich magmatic fluids. We propose a quantitative genetic model that links these crustal-scale anomalies to the formation of the IOA-IOCG deposits, and in doing so we underscore the value of MT imaging in the mineral systems framework.

* Corresponding author.
E-mail address: bmurphy@usgs.gov (B.S. Murphy).

https://doi.org/10.1016/j.epsl.2022.117700

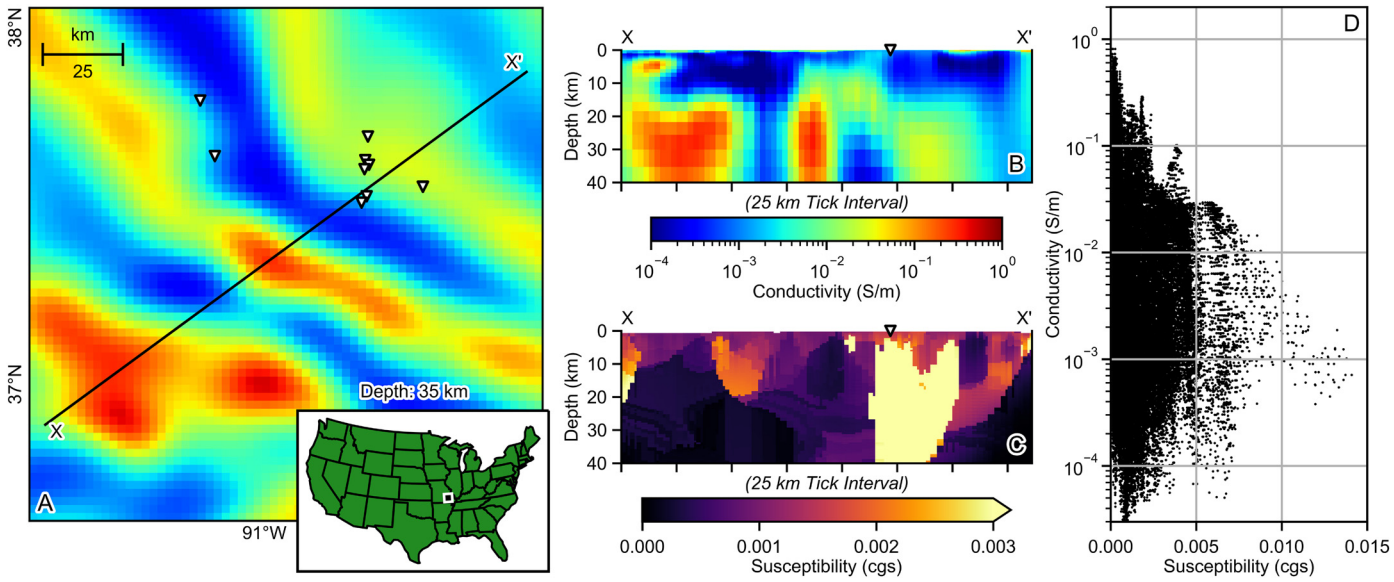

Fig. 1. Geophysical images from the Southeast Missouri Iron Province (SMIP), USA. (**A-B**) Depth slice (at 35 km depth) and cross section (roughly across the axis of extension in the SMIP; cf. DeLucia et al., 2019) through a new MT-derived electrical conductivity model (details of the inversion methodology are provided in the Supplemental Materials). Inverted triangles denote iron oxide-apatite (IOA) and iron oxide-copper-gold (IOCG) deposits. Note the moderately conductive ($\sim 10^{-2}$ S/m) "finger" that extends into the uppermost crust beneath one of these deposits in the cross section. (**C**) Cross section through the magnetic susceptibility model of McCafferty et al. (2019). The high susceptibility body in this image has been previously interpreted as the signature of a trans-crustal intrusive system. (**D**) Discrimination diagram that demonstrates the spatial relationships between imaged conductivity (A-B) and susceptibility (C). Values are sampled on a 2.5 km ×2.5 km horizontal grid across the region shown in (A) at 1 km intervals from 10-40 km depth.

2. Conductivity mechanisms

Most explanations for crustal electrical conductivity anomalies imply specific physicochemical conditions that do not match inferences for the Olympic Dam region and the SMIP. Here, we demonstrate that graphite is the only reasonable explanation, and indeed the best explanation, for the crustal-scale conductivity anomalies observed in these regions.

2.1. Free fluids

Although often invoked in tectonically active domains, deep saline fluids are implausible in the ancient intracratonic settings in which these deposits are located. Fluids associated with original tectonomagmatism would have been consumed by retrograde hydration reactions on a time scale of $\sim$ 10 Ma (e.g., Manning, 2018; Yardley and Valley, 1997; see also Yardley and Bodnar, 2014). As these regions have not experienced regional tectonism in >1 Ga, there is no modern source for deep fluid delivery into the mid-lower crust, and we consider it highly unlikely that meteoric fluids would percolate to such great depths under presumably lithostatic pressure gradients.

2.2. Metallic sulfides and oxides

Metallic sulfides (e.g., pyrite, pyrrhotite) are electrically conductive ($\sim 10^3 - 10^5$ S/m; Keller, 1966); however, we discount such phases given the available geometric and tectonic constraints. Metasedimentary pyrite has been shown to be partly responsible for conductivity anomalies in paleo-subduction settings (Jones et al., 1997), but Olympic Dam and the SMIP are not located within suture zones. Subvertical, crustal-scale sulfide zones are problematic explanations in any other tectonic setting, as unreasonably large amounts (> 10 wt%; Nelson and Van Voorhis, 1983) of intrusion-related sulfides throughout the mid-lower crust would be required to explain the observed anomalies. Although lower-crustal sulfide-rich intrusive bodies are recognized in the surface rock record (e.g., in the Ivrea Zone, northern Italy; Fiorentini et al., 2018), only locally within those intrusions does the sulfide content become high enough that a bulk conductivity anomaly ($> 10^{-1}$ S/m) would be expected (cf. Vukmanovic et al., 2019; Nelson and Van Voorhis, 1983). Therefore, we consider it highly unlikely that sulfides alone can explain the observed high conductivity values in the Olympic Dam region and in the SMIP.

Metallic oxides (e.g., magnetite, ilmenite) are similarly electrically conductive ($\sim 10^0 - 10^3$ S/m; Keller, 1966), and laboratory experiments indicate that they can become interconnected at moderate volume fractions ($\sim$ 5%) to produce a bulk conductivity anomaly (Dai et al., 2019). However, these phases also often have very high magnetic susceptibilities (cf. Hunt et al., 1995). Conductive zones beneath the SMIP are associated with domains of low magnetic susceptibility (Fig. 1D), so such phases cannot be the cause of the observed high conductivity values.

In both of these cases, relatively high volume fractions ($> 10^{-2} - 10^{-1}$) of the conductive phase at spatial scales ranging from 10s of microns (Dai et al., 2019) to 10s of meters (Nelson and Van Voorhis, 1983) are needed to enhance bulk electrical conductivity. This requirement is due to the characteristic equant habit of metallic sulfides and oxides. Only at such high concentrations can these minerals form a texturally interconnected network that can produce a conductivity anomaly.

2.3. Silicate minerals

Electrical conduction in silicate minerals is thermally activated, so these phases are incapable of producing a major electrical conductivity anomaly at the cold crustal temperatures in these stable Precambrian domains. Lower-crustal temperatures are < 600 °C at present in the SMIP (e.g., Schutt et al., 2018); at these temperatures, intrinsic semiconduction in potentially volumetrically significant silicates (e.g., feldspars, amphiboles, epidote) would produce bulk conductivity values $< 10^{-2}$ S/m (e.g., Hu et al., 2013, 2017, 2018). Extrinsic, volatile-mediated semiconduction in either micas (e.g., phlogopite) or nominally anhydrous minerals (e.g., feldspars, pyroxenes) would similarly only produce bulk conductivity values of $\sim 10^{-2}$ S/m at these cold temperatures (e.g.,

Yang et al., 2012; Li et al., 2017). Although lower-crustal temperatures in the Olympic Dam region may be somewhat higher than in the SMIP (e.g., Heinson et al., 2018), we nevertheless consider it unlikely that networks of volatile-bearing silicates can explain conductivity values $> 10^{-1}$ S/m within stable Precambrian crust, as such values would require temperatures $> 700 - 800\,^{\circ}C$ throughout the mid-lower crust.

2.4. Grain size reduction

Silicate mineral grain size diminution within high-strain shear zones enhances electrical conductivity, as ionic transport is much more efficient along grain boundaries than within grain interiors, and grain boundaries dominate bulk behavior at small (< 1 mm) grain sizes (e.g., Han et al., 2021; Pommier et al., 2018). However, the degree of conductivity enhancement depends upon temperature. Crustal conductivity values $> 10^{-1}$ S/m at grain sizes of $1 - 100$ μm (as would be expected for typical mid-lower crustal mylonitic shear zones; e.g., Okudaira et al., 2017; Waters-Tormey and Tikoff, 2007) generally require temperatures $> 800\,^{\circ}C$ (e.g., Han et al., 2021), which is unreasonable for the Olympic Dam region and the SMIP (as discussed in Section 2.3).

2.5. Graphite

Given the above considerations, graphite is the only plausible cause of these conductivity anomalies, as this phase is highly conductive ($\sim 10^6$ S/m; Keller, 1966) and can become readily interconnected at very small volume fractions due to its sheet-like habit (e.g., Glover, 1996) in order to produce a major bulk conductivity anomaly. Graphite has in fact been widely invoked in a range of settings to explain observed electrical conductivity anomalies (e.g., Evans, 2012; Glover and Ádám, 2008; Haak et al., 1997). For example, graphite is often used to explain crustal conductors in paleo-subduction settings, where biogenic carbon has been recrystallized to interconnected graphite in deformed metasedimentary rocks (e.g., Boerner et al., 1996). However, this genetic model is incompatible with tectonic inferences for the Olympic Dam region and the SMIP. Instead, we view graphite here as having precipitated from a CO_2-rich magmatically derived fluid. Such an interpretation has been qualitatively discussed previously to various extents (e.g., Monteiro Santos et al., 2002; Selway, 2014), including in the context of mineral systems (e.g., Heinson et al., 2006; Wannamaker and Doerner, 2002); however, its importance as a signature of tectonomagmatism has not been widely appreciated, and a rigorous quantitative justification for this interpretation has been critically lacking.

There are several mechanisms by which graphite may precipitate from magmatic fluids. In cooling rocks that contain titanomagnetite, the oxyexsolution reaction $6Fe_2TiO_4 + CO_2 = 2Fe_3O_4 + 6FeTiO_3 + C$ (Frost et al., 1989), where the CO_2 is derived from a magmatic fluid, is one possible means to form graphite. However, conductivity anomalies in the SMIP are spatially associated with domains of low magnetic susceptibility (Fig. 1D); this relationship suggests that there is little magnetite in the conductive zones that could have facilitated this reaction. Fluid-rock hydration reactions can also drive graphite precipitation (e.g., Rumble, 2014). Such reactions, however, are often self-limiting because the wall rock generally cannot serve as an infinite sink for water (e.g., Luque et al., 2014). Instead, we consider graphite precipitation via carbon saturation in a cooling CO_2-rich fluid to be the most likely scenario, as this mechanism does not impose any petrologic requirements upon the system and as such reactions can facilitate the precipitation of large amounts of graphite (e.g., Huizenga, 2011). This mode of graphite deposition has been well studied (e.g., Huizenga, 2011; Luque et al., 2014; and references therein) and is in fact thought to be common in the crust (Rumble, 2014). Consequently, we consider hydrothermal graphite precipitation from a cooling CO_2-rich magmatic fluid to in fact be a natural explanation for these conductivity anomalies.

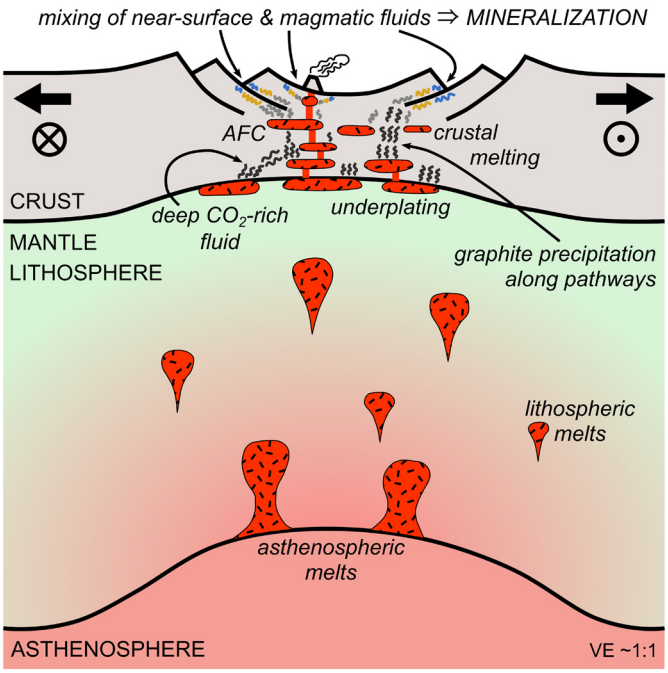

Fig. 2. Conceptual model for hydrothermal graphite precipitation beneath magmatic-hydrothermal IOA-IOCG deposits in an extensional setting (possibly with some component of lateral translation; e.g., DeLucia et al., 2019). Mantle-derived melts stall in the lower crust and exsolve a CO_2-rich fluid; as this magmatic fluid cools, it precipitates graphite. At higher crustal levels, magmatic fluids derived from more evolved melts, produced by crustal assimilation and fractional crystallization (AFC) and crustal anatexis, drive mineralization via mixing with a near-surface fluid (e.g., Barton, 2014).

3. Model for graphite precipitation

In our conceptual model (Fig. 2), graphite precipitates from migrating CO_2-rich fluids that are carried into the crust by mantle-derived melts in an extensional setting. Although carbon could be scavenged from local metasedimentary rocks, we consider the mantle as the key quantifiable source for carbon, as genetic models for these IOA-IOCG deposits invoke mantle-derived melts to establish the magmatic-hydrothermal system (McCafferty et al., 2019; Skirrow et al., 2018) and as carbon isotopes from the SMIP support the input of mantle-derived carbon (Johnson et al., 2016). In our model, graphite largely precipitates at mid- to lower-crustal levels from fluids that are exsolved from stalled mafic melts; at upper-crustal levels, fluids derived from related, more evolved melts drive IOA-IOCG mineralization via mixing with near-surface fluids.

In order to evaluate whether our conceptual model can explain the MT observations, we calculate the amplitude of the electrical conductivity anomaly that would be produced given the available carbon budget and physicochemical constraints. We summarize the three main steps of this calculation below; additional details are provided in the Supplemental Materials.

3.1. Carbon budget

First, we estimate the absolute amount of carbon that is mobilized from the mantle during magmatism. Estimates of carbon content in the upper mantle are $\sim 30 - 1000$ ppmw C (e.g., Lee et al., 2019); we conservatively assume an average content of 30

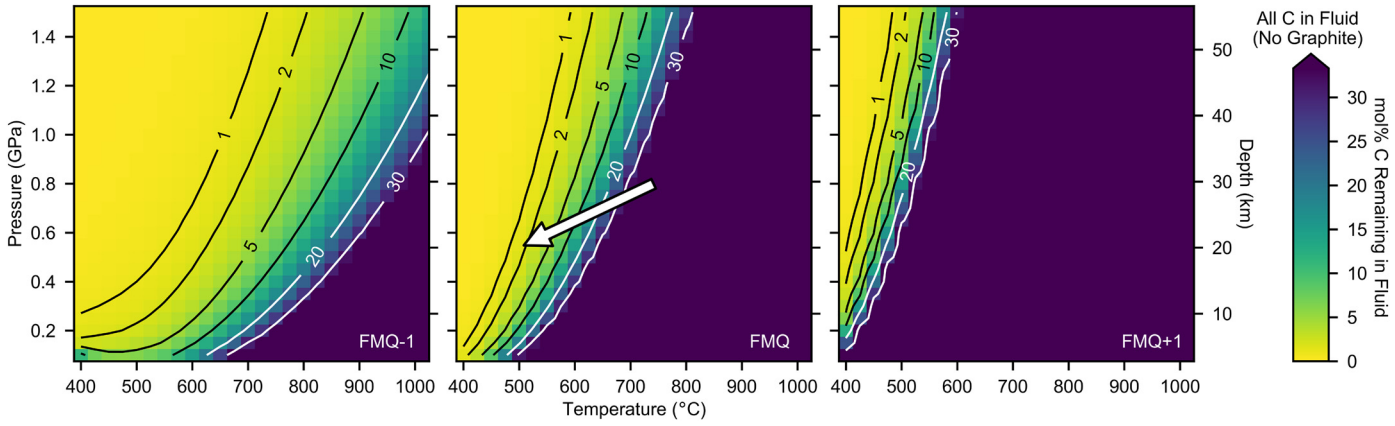

Fig. 3. Calculated relative amount of C that can be dissolved in the fluid at C saturation for a fixed f_{O_2}, expressed as log unit offset from the FMQ buffer. The maximum relative amount of C that can be dissolved in the fluid before graphite saturation is ~33.3 mol%, corresponding to nearly pure CO_2. Decreasing C content indicates that graphite precipitates out of the fluid. The arrow shows the hypothetical P/T path (25 °C/km) discussed in the text.

ppmw C. Because CO_2 is highly incompatible, we make a simplifying assumption that this full amount of C will be removed from the mantle, regardless of the degree of partial melting (e.g., Moore and Bodnar, 2019). Geodynamic modeling studies suggest an $\sim 1000-4000$ km^3 mantle source volume per kilometer of rift length (e.g., Schmeling, 2010). Taking the lower bound, we estimate that 8.24×10^{12} mol C is mobilized per kilometer along the axis of extension during mantle melting. We further conservatively assume that 10% of this available C (8.24×10^{11} mol C) will be released into the mid-lower crust via expulsion from stalled melts, while the remainder is transported with melt into near-surface volcanic systems.

3.2. Graphite precipitation

Next, we calculate the relative amount of carbon that would precipitate from the magmatic fluid under changing pressure (P) and temperature (T) conditions. We model this fluid with the system C-O-H. Although the exsolved magmatic fluid would likely be saline, immiscibility at high P/T yields two separate fluids, a CO_2-rich fluid and a hypersaline brine, that would evolve separately (e.g., Manning, 2018; Yardley and Bodnar, 2014). The C-O-H fluid is therefore a useful approximation for our purposes here. We use the GFluid spreadsheet (Zhang and Duan, 2010), modified to use the fayalite-magnetite-quartz (FMQ) oxygen fugacity (f_{O_2}) buffer of Ballhaus et al. (1991), to calculate the maximum relative amount of C at saturation (i.e., fluid C activity is unity) that can be retained in the fluid as a function of P/T. In these calculations, we assume that the wall rock serves as a sink for O_2 so that the fluid is held at constant f_{O_2} during graphite precipitation. (If O_2 instead remains in the fluid, then fluid f_{O_2} will increase during graphite precipitation, and the net graphite precipitation potential will then be less than with constant fluid f_{O_2}; Huizenga, 2011. However, the wall rock is expected to buffer the fluid to constant f_{O_2}; Selverstone, 2005.)

The results of these calculations are shown in Fig. 3. In these plots, the fractional difference between any two points gives the relative amount of C that is precipitated out of (or dissolved into) the fluid under changing P/T conditions. The fluid becomes saturated in C with decreasing T and will then precipitate graphite, which leads to the C decrease in the fluid shown in these plots. We assume a hypothetical P/T path (arrow in Fig. 3) representing fluid migration out of the lower crust to higher crustal levels, with the fluid cooling along an approximate average crustal geotherm during tectonomagmatism. (Although magmatic intrusions will modulate the crustal thermal field, we expect that this path will generally capture the average P/T changes experienced during fluid flow. Furthermore, although migrating fluids will advect heat to some extent, they generally shed much of that heat to reach thermal equilibrium with the rocks through which they pass; e.g., Ague, 2014.) We further assume that the mantle source region sets fluid f_{O_2} to ~FMQ; this value is reasonable for the upper mantle, even in subduction-modified settings (Frost and McCammon, 2008). Igneous zircon-hosted iron oxide inclusions from the SMIP also provide supporting evidence that redox conditions of ore-stage magmas were near FMQ (Watts and Mercer, 2020). (The IOA-IOCG deposits themselves are more oxidized due, at least in part, to fluid mixing.) For this assumed P/T path, 96% of the C in the magmatic fluid is precipitated as graphite.

3.3. Resulting conductivity anomaly

Finally, we evaluate the magnitude of the conductivity anomaly that would be produced by graphite precipitation from the magmatic fluid. Combining our absolute C budget estimate (Section 3.1) with our calculated relative amount of C precipitated along the assumed P/T path (Section 3.2), we conclude that 7.89×10^{11} mol C is precipitated as graphite during magmatic fluid migration. We assume that the graphite is distributed over an area of 100 km across the axis of extension (based on the region of maximum surface deformation during extension from geodynamic modeling studies; e.g., Schmeling, 2010) by 10 km in depth (reflecting the arrow in Fig. 3), per kilometer along the axis of extension. This would produce a bulk graphite volume fraction of 4.16×10^{-6}. Although the precipitated graphite would likely be concentrated along discrete permeable fluid pathways (either tectonically controlled or created by fluid overpressurization), this value reflects an overall bulk-average volume fraction across this model domain. In order to evaluate the expected magnitude of the resulting electrical conductivity anomaly, we then compare this value to various two-component mixing laws between electrically resistive rock-forming silicate minerals and electrically conductive graphite in Fig. 4.

The key curves in Fig. 4 are the Hashin-Shtrikman (HS) bounds, which provide the most general upper and lower limits on the bulk electrical conductivity of a two-component mixture (Hashin and Shtrikman, 1962; see also Schmeling, 1986). The upper conductivity bound reflects a system in which the more conductive phase (in this case, graphite) is texturally well connected, whereas the lower conductivity bound reflects a geometry in which the more conductive phase is poorly connected. The other mixing laws shown in Fig. 4 reflect specific textural geometries of the two phases, with curves plotting near the upper HS conductivity bound reflecting geometries in which the more conductive phase is generally interconnected. In comparing our calculated volume fraction to these

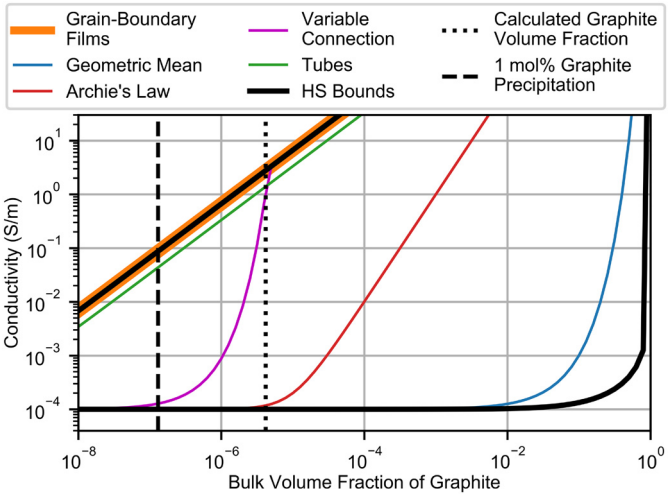

Fig. 4. Calculated electrical conductivity as a function of graphite volume fraction for various two-component mixing laws (Schmeling, 1986; graphite: 10^6 S/m, Keller, 1966; crystalline silicate crust: 10^{-4} S/m). Vertical dotted/dashed lines denote graphite volume fractions discussed in the text. Mixing laws near the upper Hashin-Shtrikman (HS) conductivity bound reflect systems in which the conductive phase is well interconnected; mixing laws near the lower HS conductivity bound reflect systems in which the conductive phase is poorly interconnected.

mixing laws, the degree of textural interconnection is the crucial factor that dictates whether such small amounts of graphite will enhance bulk electrical conductivity. As Fig. 4 demonstrates, if the precipitated graphite in our model is indeed well connected, such that it is characterized by the upper conductivity bound, then our calculated bulk-average graphite volume fraction of 4.16×10^{-6} (and even bulk volume fractions an order of magnitude less than this value) will produce a conductivity anomaly comparable to what is observed beneath these IOA-IOCG deposits ($\sim 10^0$ S/m).

The graphite will indeed likely be well connected when precipitated from a mobile fluid along permeable pathways. Although CO_2-rich fluids themselves are not expected to be readily mobile due to poor grain-boundary wetting (e.g., Manning, 2018), their mobility will be greatly enhanced by the additional presence of saline fluids (e.g., Newton and Tsunogae, 2014; Touret et al., 2019) that are common in magmatic systems (e.g., Pirajno, 2021; Yardley and Bodnar, 2014). Therefore, the related exsolved magmatic saline fluid in our model that results from fluid immiscibility (see Section 3.2) will promote mobility of the CO_2-rich fluid and, consequently, interconnection of the precipitated graphite. (Regardless of the coexistence of saline fluids, observations of passive CO_2 degassing in extensional settings indicates that such CO_2-rich fluids are nevertheless mobile via some mechanism through the crust; Tamburello et al., 2018.) Syngenetic shearing of tectonically controlled fluid pathways could act to further promote interconnection (e.g., Jödicke et al., 2004).

4. Discussion

4.1. Implications for regional mineral exploration

Our purposefully conservative calculations here validate the inference that electrical conductivity anomalies, in the correct tectonic setting, may demarcate zones of crustal-scale magmatic fluid flow. However, there are many ways to produce a conductivity anomaly (as discussed in Section 2), and not all anomalies will be linked to ore mineralization. Complementary geological, geochemical, and geophysical observations are needed to determine whether hydrothermal graphite precipitation may be a reasonable interpretation for a given feature in an MT image that could then provide a link to a prospective magmatic or magmatic-hydrothermal mineral system.

It is crucial to note that these conductors are specifically associated with the roots of a potential mineral system in our model and therefore may be only indirectly related to ore mineralization. Although CO_2-rich fluids may play a key role in transporting metals from the mantle into the crust (Blanks et al., 2020) and may be important in producing alteration patterns within IOA-IOCG deposits (e.g., Pirajno, 2021), we lack direct evidence that can link the deep CO_2-rich fluids in our model to ore-forming processes operating at higher crustal levels. Consequently, the fluids that precipitate graphite in our model are not necessarily the same fluids that carry metals into the mineral system. Indeed, the magmatic fluids that precipitate graphite are almost certainly not directly the same as those that drive ore mineralization; formation of mineral deposits at upper crustal depths is likely the result of mixing between more evolved magmatic fluids, derived from more evolved melts, and near-surface fluids (Fig. 2; Barton, 2014; Schlegel et al., 2020). Consequently, in our model, graphite precipitation and mineral deposit formation are two independent components of a single mineral system. When combined with other datasets to constrain tectonic setting, MT-imaged conductivity anomalies may then be indicative of a paleo-tectonomagmatic system that could have driven ore mineralization at upper crustal levels.

Furthermore, as graphite precipitation and mineral deposit formation occur in disparate crustal intervals within the overall mineral system, there should be no expectation that the graphite that causes these mid-lower crustal conductivity anomalies will be significantly exposed in the upper crust, at the deposit or even regional district scale. Although this mismatch in crustal levels presents a challenge in validating our model, examination of exposed lower crustal sections may provide valuable insights in assessing the role of hydrothermal graphite precipitation in mineral systems (see Section 4.4).

4.2. Redox requirements and implications

Although we have purposefully made conservative estimates in our C budget calculations, our results are dependent upon the redox conditions of the magmatic fluid. The C mol% isopleths in Fig. 3 change significantly when moving away from the FMQ buffer. The distribution of these isopleths determines both the depth at which graphite will precipitate from the fluid (based on P/T conditions through the crust) and how much cooling is required to precipitate a fixed amount of graphite (more reduced conditions require more cooling for the same C precipitation). However, if the fluid f_{O_2} were to deviate significantly from FMQ, even precipitating just 3% of the available C (1 mol% of fluid C) still results in a significant bulk conductivity anomaly ($\sim 10^{-1}$ S/m, compared to $\sim 10^{-4}$ S/m crystalline crustal background; Fig. 4), as long as the graphite is texturally interconnected. (Similarly, if fluid f_{O_2} were to increase during graphite precipitation due to violation of our assumptions in Section 3.2, an order of magnitude less graphite would still yield a bulk conductivity anomaly comparable to what is observed in Fig. 1.)

The highest amplitude portions of the observed anomalies beneath Olympic Dam and in the SMIP generally appear to be restricted to a certain depth range (e.g., Fig. 1; Heinson et al., 2018). Although it has been suggested that the tops of these conductors reflect the brittle-ductile transition at the time of mineral system formation (e.g., Heinson et al., 2018), we consider it more likely that this pattern reflects the spatial location of P/T conditions that were most conducive for graphite precipitation from the magmatic fluid—i.e., in Fig. 3, the P/T field over which the fluid C content drops rapidly from ~ 30 to ~ 1 mol%. If the redox conditions of the magmatic fluid can be estimated, then the depth range of these

conductors may provide constraints on paleo P/T conditions during fluid flow with implications for mineral exploration efforts. Alternatively, if paleo P/T conditions can be independently constrained, then the depth extent of these features may provide insights into magmatic redox conditions.

4.3. Graphite volume fractions and the scale of interconnection

In order to produce a bulk electrical conductivity anomaly comparable to observations, the small (4.16×10^{-6}) bulk-average volume fraction of graphite that we calculate here must be interconnected across our model domain. Laboratory experiments indicate that graphite volume fractions as high as $\sim 10^{-2} - 10^{-1}$ are insufficient to enhance bulk electrical conductivity due to poor interconnection of the conductive phase (e.g., Hashim et al., 2013; Jödicke et al., 2007; Wang et al., 2013; Zhang and Yoshino, 2017). However, such experiments have often focused on biogenic carbon in metasedimentary rocks and graphite in synthetic crystal aggregates; few laboratory observations have been made specifically on rocks containing fluid-precipitated graphite. Where laboratory experiments indicate low electrical conductivity ($< 10^{-3}$ S/m) for rocks that do contain hydrothermal graphite, the low values are suggested to be an artifact due to disruption of the graphite electrical connection during rock exhumation (e.g., Katsube and Mareschal, 1993). Laboratory observations of increasing electrical conductivity with increasing pressure in metamorphic rocks containing small amounts ($< 10^{-2}$ volume fraction) of fluid-precipitated graphite (Mathez et al., 1995; Shankland et al., 1997) suggest that small volume fractions of this conductive phase can indeed contribute to enhanced electrical conductivity under realistic crustal physicochemical conditions.

A key complication in comparing laboratory experiments to geophysical imaging results, however, is the intrinsic mismatch between observation scales. Laboratory experiments at the hand-sample scale ($\sim$ 10s of cm) struggle to capture the bulk crustal properties that would be expected when averaging over the large scales ($\sim$ 10s of m to several km) at which geophysical imaging techniques such as MT aggregate information (e.g., Bahr, 1997). For example, in the MT images of the SMIP shown in Fig. 1, the nominal horizontal cell size in the inversion is 2.5 km by 2.5 km (see the Supplemental Materials). In this case, electrical conductivity information is inherently bulk averaged over that length scale (at a minimum; regularization, survey design, and variable electromagnetic diffusion further increase this averaging length scale). Consequently, within such large averaging volumes, the actual distribution of graphite is unconstrained. Fig. 5 demonstrates the equivalence between homogeneously low and heterogeneously high graphite concentrations to yield the same observed bulk electrical conductivity value within a given averaging volume. For example, the same bulk-average electrical conductivity ($\sim 2.7 \times 10^{0}$ S/m) would arise for either the entire averaging volume containing a graphite volume fraction of 4.16×10^{-6} or for a fraction of 4.16×10^{-6} of the total averaging volume containing veins of pure (volume fraction 10^{0}) graphite (these are endmembers of the thick dotted line in Fig. 5). Near-surface electrical observations of the spatial distribution of graphite in exposed mid-lower crustal rocks in Norway (Engvik et al., 2021) and Sri Lanka (Wickramasinghe et al., 2018) confirm that zones of graphite enrichment ($> 10^{-1}$ volume fraction, with electrical conductivity $> 10^{-1}$ S/m) are highly heterogeneously distributed, but variably laterally connected, at the scale of 100s of meters to 10s of kilometers.

In our model, we envision graphite deposition occurring along discrete permeable fluid-flow pathways. Sections of the crust along these pathways would then be enriched in graphite compared to our calculated overall bulk-average graphite volume fraction (likely by orders of magnitude), whereas sections of the crust outside of these pathways would be largely devoid of graphite. Large-scale electrical interconnection of discrete, graphite-enriched permeable pathways would likely be characterized by the upper HS conductivity bound, as we expect these pathways to be texturally well connected at large scales given that they facilitate fluid flow. Consequently, despite the aforementioned ambiguities in laboratory observations, we consider it likely that the small overall bulk-average volume fraction of fluid-precipitated graphite that we calculate in Section 3.3 will texturally be characterized by the upper HS conductivity bound at the large scales at which geophysical observations aggregate information. We then expect the resulting bulk-average conductivity values to match MT observations.

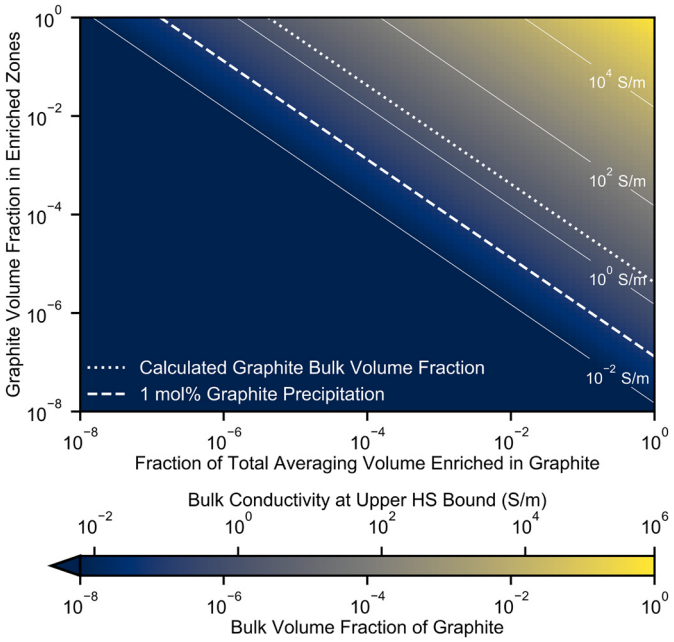

Fig. 5. Bulk mixing relationship between the fraction of the total geophysical averaging volume that is enriched in the conductive phase (in this case, graphite) and the concentration of the conductive phase within those enrichment zones. Diagonal lines of constant bulk-average volume fraction demonstrate the equivalence of various distributions of the conductive phase within the geophysical averaging volume. Thick dotted and dashed lines denote the bulk volume fractions calculated and discussed in Sections 3.3 and 4.2 (and also shown in Fig. 4). Thin solid lines are labeled with the equivalent electrical conductivity value that would be expected for the resulting constant bulk-averaged graphite volume fraction, assuming the graphite is well connected and can be described by the upper Hashin-Shtrikman (HS) conductivity bound.

4.4. Potential analogs in the surface rock record

Along the permeable fluid pathways in our model, we envision graphite precipitating either as grain-boundary films or in a crustal-scale network of graphite veins. Grain-boundary graphite films have long been recognized in mid-lower crustal rocks (e.g., Frost et al., 1989; Mareschal et al., 1992); however, laboratory experiments are inconsistent in demonstrating the effects of such films in enhancing bulk electrical conductivity. Older laboratory experiments have provided evidence that graphite films do enhance bulk conductivity to some extent when held at mid-crustal pressures that would keep graphite networks interconnected (Mathez et al., 1995; Shankland et al., 1997), and experiments with vapor-deposited graphite films similarly support an enhancement of conductivity at low volume fractions (Roberts et al., 1999). However, newer laboratory experiments indicate that thin (< 1 µm) graphite films are unstable at high temperatures (> 700 °C; Yoshino and Noritake, 2011) and over long time scales ($>$ 10s of ka). Given these competing laboratory results, we conclude that cooling

and crustal "fossilization" could promote the stability of thicker (> 1 μm) grain-boundary films, and the persistence of an associated conductivity anomaly, over long geologic time scales. Because there is no evidence for major post-ore tectonomagmatism in either the Olympic Dam region or the SMIP, and because mid-lower crustal temperatures in these regions are generally $< 700\,^{\circ}$C at present (see Section 2.3), we consider grain-boundary films to be a feasible textural model for the occurrence of graphite in these domains, particularly within ancient fluid-flow pathways where thick (> 1 μm) grain-boundary films would be expected.

However, we consider it more likely that the graphite in these regions occurs within interconnected vein networks, as this mode of occurrence is widely recognized in the rock record (e.g., Luque et al., 2014). In particular, the Sri Lankan vein graphite deposits (e.g., Touret et al., 2019) may provide an analog for what lies beneath the Olympic Dam region and the SMIP. The Sri Lankan graphite is inferred to have formed from mantle-derived carbon-rich fluids, similar to what we envision here within these mineral systems. The Sri Lankan deposits contain large volumes of graphitic carbon; based on local geologic mapping (Erdosh, 1970) and near-surface electrical observations (Wickramasinghe et al., 2018), volumetric ratios of graphite to country rock are $\sim 10^{-4}$ in the vicinity of vein deposits, roughly two orders of magnitude greater than the volume fraction we calculate in our model. However, graphite veins are irregularly distributed along the ~ 500 km corridor in which they are found in Sri Lanka (e.g., Touret et al., 2019). When averaged over larger areas, the bulk volume fraction of graphite may be comparable to that predicted by our model, particularly given the conservative assumptions underlying our calculations. Given these considerations, we view the Sri Lankan graphite veins as a promising analog for the occurrence of graphite beneath Olympic Dam and the SMIP.

Although our calculations in Section 3 apply most directly to high conductivity anomalies in the mid-lower crust, observed moderately conductive "fingers" in the upper crust (e.g., Fig. 1; Heinson et al., 2018) can perhaps also be explained by hydrothermal graphite precipitation. The Borrowdale graphite deposit in the U.K. (e.g., Luque et al., 2014) may be a reasonable analog for these conductive features. At Borrowdale, upper-crustal magmas assimilated large volumes of crustal carbon. Magmatic exsolution and consequent overpressurization of carbon-rich fluids, with redox conditions at or just above the FMQ buffer, caused brecciation of the host rock; graphite was then precipitated from these fluids during pervasive wall-rock hydration reactions. Although there is no evidence for the magmatic remobilization of crustal carbon in either the Olympic Dam region or the SMIP, evolved upper-crustal magmatic fluids in these regions could have still carried enough mantle-derived carbon at the appropriate redox conditions to precipitate graphite via hydration reactions at shallow depths (i.e., during propylitic alteration of the country rock immediately below the IOA-IOCG deposits) and to thereby yield a moderate conductivity ($\sim 10^{-2}$ S/m) anomaly at such depths. These upper-crustal "fingers" may be further enhanced or alternatively explained by sulfide vein mineralization or hydrothermal clays associated with wall-rock alteration (e.g., Delayre et al., 2020).

4.5. Application to other mineral systems

The viability of using electrically conductive hydrothermal graphite to identify the roots of magmatic-hydrothermal mineral systems more broadly will be dictated by the redox requirements for graphite precipitation. Although graphite will readily precipitate from a fluid with redox conditions near (within one log unit of) or below the FMQ buffer, graphite is not expected to precipitate from a fluid at more than two log units above the FMQ buffer (e.g., Huizenga, 2011). Consequently, hydrothermal graphite precipitation is unlikely in porphyry copper systems, as the magmas and associated mid-lower crustal magmatic fluids are generally highly oxidized with respect to FMQ (e.g., Lee and Tang, 2020). Hydrothermal graphite will likely only be present in mineral systems characterized by magmatic redox conditions near FMQ.

Similarly, our model may not apply to all IOA-IOCG systems, as such deposits form through many different mechanisms in a range of tectonic settings (e.g., Barton, 2014; Schlegel et al., 2020). Not all IOA-IOCG formation mechanisms involve the mobilization of deep CO_2-rich fluids that could precipitate graphite, and other conductivity mechanisms (cf. Section 2) may explain observations, depending on tectonic setting. For example, a major conductivity anomaly is observed beneath the Ernest Henry IOCG deposit in the Cloncurry District, Australia (Jiang et al., 2019; Wang et al., 2018). That deposit likely formed, at least partially, in an orogenic setting (e.g., Barton, 2014), so underthrust conductive metasedimentary units (e.g., Boerner et al., 1996; Jones et al., 1997) may provide an alternative explanation for the observed anomaly.

Although we have specifically argued for mantle-derived carbon in our model, it is nevertheless possible that remobilization and reprecipitation of crustal carbon through mechanisms similar to those that we have argued for here (e.g., Luque et al., 2014) may also produce a regional-scale conductivity anomaly. Magmatic assimilation of carbonaceous material and subsequent exsolution of carbon-rich fluids may ultimately drive hydrothermal graphite precipitation that could yield a conductivity anomaly within a mineral system. Additionally, because crustal carbon can act as a reducing agent during magmatic assimilation, hydrothermal graphite precipitation from fluids associated with such hybridized magmas may be a useful geophysical tracer for studying systems in which magmatic redox processes are key for mineral system evolution (e.g., in certain reduced gold systems, such as gold porphyries and possibly Carlin-type/-like systems; Johnson et al., 2020).

5. Conclusions

We have quantitatively demonstrated that graphite precipitation from CO_2-rich magmatically derived fluids is the best explanation for the crustal-scale electrical conductivity anomalies observed beneath the Olympic Dam region and the SMIP. Furthermore, hydrothermal graphite is a natural explanation for these anomalies, as graphite will readily precipitate from carbon-bearing fluids throughout the crustal column either via cooling or via hydration reactions, under reasonable fluid redox constraints. The physicochemical principles upon which our model is based can consequently be readily extended to other magmatic-hydrothermal mineral systems, provided that there is a source of carbon (either from the mantle or from the crust) and that the magmatic fluid redox conditions are appropriate for graphite precipitation. Hydrothermal graphite may then be a useful electrically conductive indicator of ancient crustal-scale fluid flow and a valuable crustal-scale vector in exploring for magmatic-hydrothermal ore deposits.

CRediT authorship contribution statement

Benjamin S. Murphy: Conceptualization, Investigation, Methodology, Writing – original draft. **Jan Marten Huizenga:** Investigation, Methodology, Validation, Writing – review & editing. **Paul A. Bedrosian:** Investigation, Writing – review & editing.

Declaration of competing interest

The authors declare that they have no known competing financial interests or personal relationships that could have appeared to influence the work reported in this paper.

Data availability

The MT data used in this study are available from the IRIS EMTF database (Kelbert et al., 2011; http://ds.iris.edu/spud/emtf). The MT-derived conductivity model shown in Fig. 1 is available from the IRIS EMC (http://ds.iris.edu/ds/products/emc/).

Acknowledgements

We thank Fabrice Gaillard, Kate Selway, and an anonymous reviewer for constructive reviews of this manuscript, and we thank editor Rajdeep Dasgupta for facilitating journal review of this work. We also thank Al Hofstra, Krissy Lewis, Brian Shiro, Meredith Nevers, and Janet Slate for internal review of this manuscript. Numerous conversations with Al Hofstra and John Dilles greatly benefited this work. We thank Anne Fulton for feedback on preliminary versions of this manuscript and Nikki Moore for valuable input on aspects of our calculations. BSM is supported by a Mendenhall Postdoctoral Fellowship through the U.S. Geological Survey. Any use of trade, firm, or product names is for descriptive purposes only and does not imply endorsement by the U.S. Government.

Appendix A. Supplementary material

Supplementary material related to this article can be found online at https://doi.org/10.1016/j.epsl.2022.117700.

References

Ague, J.J., 2014. 4.6 - Fluid Flow in the Deep Crust. In: Holland, H.D., Turekian, K.K.B.T.-T. (Eds.), second e. Elsevier, Oxford, pp. 203–247.

Bahr, R., 1997. Electrical anisotropy and conductivity distribution functions of fractal random networks and of the crust: the scale effect of connectivity. Geophys. J. Int. 130, 649–660. https://doi.org/10.1111/j.1365-246X.1997.tb01859.x.

Ballhaus, C., Berry, R.F., Green, D.H., 1991. High pressure experimental calibration of the olivine-orthopyroxene-spinel oxygen geobarometer: implications for the oxidation state of the upper mantle. Contrib. Mineral. Petrol. 107, 27–40. https://doi.org/10.1007/BF00311183.

Barton, M.D., 2014. Iron Oxide(-Cu-Au-REE-P-Ag-U-Co) Systems, 2nd ed. Treatise on Geochemistry: Second Edition. Elsevier Ltd.

Blanks, D.E., Holwell, D.A., Fiorentini, M.L., Moroni, M., Giuliani, A., Tassara, S., González-Jiménez, J.M., Boyce, A.J., Ferrari, E., 2020. Fluxing of mantle carbon as a physical agent for metallogenic fertilization of the crust. Nat. Commun. 11. https://doi.org/10.1038/s41467-020-18157-6.

Boerner, D.E., Kurtz, R.D., Craven, J.A., 1996. Electrical conductivity and Paleo-Proterozoic foredeeps. J. Geophys. Res. 101.

Dai, L., Hu, H., Sun, W., Li, H., Liu, C., Wang, M., 2019. Influence of high conductive magnetite impurity on the electrical conductivity of dry olivine aggregates at high temperature and high pressure. Minerals 9. https://doi.org/10.3390/min9010044.

Day, W.C., Slack, J.F., Ayuso, R.A., Seeger, C.M., 2016. Regional geologic and petrologic framework for iron oxide ± apatite ± rare earth element and iron oxide copper-gold deposits of the Mesoproterozoic St. Francois Mountains Terrane, Southeast Missouri, USA. Econ. Geol. 111, 1825–1858. https://doi.org/10.2113/econgeo.111.8.1825.

Delayre, C., Mas, P.P., Sardini, P., Cosenza, P., Thomas, A., 2020. Quantitative evolution of the petrophysical properties of andesites affected by argillic alteration in the hydrothermal system of Petite Anse-Diamant, Martinique. J. Volcanol. Geotherm. Res. 401, 106927. https://doi.org/10.1016/j.jvolgeores.2020.106927.

DeLucia, M.S., Murphy, B.S., Marshak, S., Egbert, G.D., 2019. The Missouri High-Conductivity Belt, revealed by magnetotelluric imaging: evidence of a trans-lithospheric shear zone beneath the Ozark Plateau, Midcontinent USA? Tectonophysics 753, 111–123. https://doi.org/10.1016/j.tecto.2019.01.011.

Engvik, A.K., Gautneb, H., Baranwal, V.C., Rønning, J.S., Knežević Solberg, J., Liu, Y., Austrheim, H., 2021. The control of shear-zone development and electric conductivity by graphite in granulite: an example from the Proterozoic Lofoten-Vesterålen Complex of northern Norway. Terra Nova 33, 529–539. https://doi.org/10.1111/ter.12545.

Erdosh, G., 1970. Geology of bogala mine, ceylon and the origin of vein-type graphite. Miner. Depos. 5, 375–382. https://doi.org/10.1007/BF00206734.

Evans, R.L., 2012. Conductivity of Earth materials. In: Chave, A.D., Jones, A.G. (Eds.), The Magnetotelluric Method: Theory and Practice. Cambridge University Press, Cambridge, pp. 50–95.

Fiorentini, M.L., LaFlamme, C., Denyszyn, S., Mole, D., Maas, R., Locmelis, M., Caruso, S., Bui, T.H., 2018. Post-collisional alkaline magmatism as gateway for metal and sulfur enrichment of the continental lower crust. Geochim. Cosmochim. Acta 223, 175–197. https://doi.org/10.1016/j.gca.2017.11.009.

Frost, B.R., Fyfe, W.S., Tazaki, K., Chan, T., 1989. Grain-boundary graphite in rocks and implications for high electrical conductivity in the lower crust. Nature 340, 134–136. https://doi.org/10.1038/340134a0.

Frost, D.J., McCammon, C.A., 2008. The redox state of Earth's mantle. Annu. Rev. Earth Planet. Sci. 36, 389–420. https://doi.org/10.1146/annurev.earth.36.031207.124322.

Glover, P.W.J., 1996. Graphite and electrical conductivity in the lower continental crust: a review. Phys. Chem. Earth 21, 279–287. https://doi.org/10.1016/S0079-1946(97)00049-9.

Glover, P.W.J., Ádám, A., 2008. Correlation between crustal high conductivity zones and seismic activity and the role of carbon during shear deformation. J. Geophys. Res., Solid Earth 113. https://doi.org/10.1029/2008JB005804.

Haak, V., Simpson, F., Bahr, K., Bigalke, J., Eisel, M., Harms, U., Hirschmann, G., Huenges, E., Jödicke, H., Kontny, A., Kück, J., Nover, G., Rauen, A., Stoll, J., Walther, J., Winter, H., Zulauf, G., Wolfgang, J., 1997. KTB and the electrical conductivity of the crust. J. Geophys. Res., Solid Earth 102, 18289–18305. https://doi.org/10.1029/96JB03861.

Han, K., Guo, X., Zhang, J., Wang, X., Clark, S.M., 2021. Fast grain-boundary ionic conduction in multiphase aggregates as revealed by electrical conductivity measurements. Contrib. Mineral. Petrol. 176, 1–19. https://doi.org/10.1007/s00410-021-01841-1.

Hashim, L., Gaillard, F., Champallier, R., Le Breton, N., Arbaret, L., Scaillet, B., 2013. Experimental assessment of the relationships between electrical resistivity, crustal melting and strain localization beneath the Himalayan–Tibetan Belt. Earth Planet. Sci. Lett. 373, 20–30. https://doi.org/10.1016/j.epsl.2013.04.026.

Hashin, Z., Shtrikman, S., 1962. A variational approach to the theory of the effective magnetic permeability of multiphase materials. J. Appl. Phys. 33, 3125–3131. https://doi.org/10.1063/1.1728579.

Heinson, G., Didana, Y., Soeffky, P., Thiel, S., Wise, T., 2018. The crustal geophysical signature of a world-class magmatic mineral system. Sci. Rep. 8, 1–6. https://doi.org/10.1038/s41598-018-29016-2.

Heinson, G.S., Direen, N.G., Gill, R.M., 2006. Magnetotelluric evidence for a deep-crustal mineralizing system beneath the Olympic Dam iron oxide copper-gold deposit, southern Australia. Geology 34, 573–576. https://doi.org/10.1130/G22222.1.

Hu, H., Dai, L., Li, H., Hui, K., Sun, W., 2017. Influence of dehydration on the electrical conductivity of epidote and implications for high-conductivity anomalies in subduction zones. J. Geophys. Res., Solid Earth 122, 2751–2762. https://doi.org/10.1002/2016JB013767.

Hu, H., Dai, L., Li, H., Sun, W., Li, B., 2018. Effect of dehydrogenation on the electrical conductivity of Fe-bearing amphibole: Implications for high conductivity anomalies in subduction zones and continental crust. Earth Planet. Sci. Lett. 498, 27–37. https://doi.org/10.1016/j.epsl.2018.06.003.

Hu, H., Li, H., Dai, L., Shan, S., Zhu, C., 2013. Electrical conductivity of alkali feldspar solid solutions at high temperatures and high pressures. Phys. Chem. Miner. 40, 51–62. https://doi.org/10.1007/s00269-012-0546-4.

Huizenga, J.M., 2011. Thermodynamic modelling of a cooling C-O-H fluid-graphite system: Implications for hydrothermal graphite precipitation. Miner. Depos. 46, 23–33. https://doi.org/10.1007/s00126-010-0310-y.

Hunt, C.P., Moskowitz, B.M., Banerjee, S.K., 1995. Magnetic properties of rocks and minerals. In: Rock Phys. Phase Relations. In: AGU Reference Shelf.

Jiang, W., Korsch, R.J., Doublier, M.P., Duan, J., Costelloe, R., 2019. Mapping deep electrical conductivity structure in the Mount Isa region, Northern Australia: implications for mineral prospectivity. J. Geophys. Res., Solid Earth 124, 10655–10671. https://doi.org/10.1029/2019JB017528.

Jödicke, H., Kruhl, J.H., Ballhaus, C., Giese, P., Untiedt, J., 2004. Syngenetic, thin graphite-rich horizons in lower crustal rocks from the Serre San Bruno, Calabria (Italy), and implications for the nature of high-conducting deep crustal layers. Phys. Earth Planet. Inter. 141, 37–58. https://doi.org/10.1016/j.pepi.2003.09.013.

Jödicke, H., Nover, G., Kruhl, J.H., Markfort, R., 2007. Electrical properties of a graphite-rich quartzite from a former lower continental crust exposed in the Serre San Bruno, Calabria (southern Italy). Phys. Earth Planet. Inter. 165, 56–67. https://doi.org/10.1016/j.pepi.2007.08.001.

Johnson, C., Ressel, M., Ruprecht, P., 2020. Toward a global carlin-type exploration model: the relationship between Eocene magmatism and diverse gold-rich deposits in the Great Basin, USA. In: Vision for Discovery: Geological Society of Nevada Symposium Proceedings.

Johnson, C.A., Day, W.C., Rye, R.O., 2016. Oxygen, hydrogen, sulfur, and carbon isotopes in the pea ridge magnetite-apatite deposit, Southeast Missouri, and sulfur isotope comparisons to other iron deposits in the region. Econ. Geol. 111, 2017–2032. https://doi.org/10.2113/econgeo.111.8.2017.

Jones, A.G., Katsube, T.J., Schwann, P., 1997. The longest conductivity anomaly in the world explained: sulphides in fold hinges causing very high electrical anisotropy. J. Geomagn. Geoelectr. 49, 1619–1629. https://doi.org/10.5636/jgg.49.1619.

Katsube, T.J., Mareschal, M., 1993. Petrophysical model of deep electrical conductors: graphite lining as a source and its disconnection due to uplift. J. Geophys. Res., Solid Earth 98, 8019–8030. https://doi.org/10.1029/92JB02864.

Kelbert, A., Egbert, G.D., Schultz, A., 2011. IRIS DMC data services products: EMTF, the magnetotelluric transfer functions. https://doi.org/10.17611/DP/EMTF.1.

Keller, G.V., 1966. Section 26: electrical properties of rocks and minerals*. In: Clark Jr., S.P. (Ed.), Handbook of Physical Constants. Geological Society of America.

Lee, C.-T.A., Jiang, H., Dasgupta, R., Torres, M., 2019. A framework for understanding whole-Earth carbon cycling, deep carbon. https://doi.org/10.1017/9781108677950.011.

Lee, C.T.A., Tang, M., 2020. How to make porphyry copper deposits. Earth Planet. Sci. Lett. 529, 115868. https://doi.org/10.1016/j.epsl.2019.115868.

Li, Y., Jiang, H., Yang, X., 2017. Fluorine follows water: effect on electrical conductivity of silicate minerals by experimental constraints from phlogopite. Geochim. Cosmochim. Acta 217, 16–27. https://doi.org/10.1016/j.gca.2017.08.020.

Luque, F.J., Huizenga, J.M., Crespo-Feo, E., Wada, H., Ortega, L., Barrenechea, J.F., 2014. Vein graphite deposits: geological settings, origin, and economic significance. Miner. Depos. 49, 261–277. https://doi.org/10.1007/s00126-013-0489-9.

Manning, C.E., 2018. Fluids of the lower crust: deep is different. Annu. Rev. Earth Planet. Sci. 46, 67–97. https://doi.org/10.1146/annurev-earth-060614-105224.

Mareschal, M., Fyfe, W.S., Percival, J., Chan, T., 1992. Grain-boundary graphite in Kapuskasing gneisses and implications for lower-crustal conductivity. Nature 357, 674–676. https://doi.org/10.1038/357674a0.

Mathez, E.A., Duba, A.G., Peach, C.L., Leger, A., Shankland, T.J., Plafker, G., 1995. Electrical conductivity and carbon in metamorphic rocks of the Yukon- Tanana Terrane, Alaska. J. Geophys. Res. 100. https://doi.org/10.1029/95jb00615.

McCafferty, A.E., Phillips, J.D., Hofstra, A.H., Day, W.C., 2019. Crustal architecture beneath the southern Midcontinent (USA) and controls on Mesoproterozoic iron-oxide mineralization from 3D geophysical models. Ore Geol. Rev. 111. https://doi.org/10.1016/j.oregeorev.2019.102966.

McCuaig, T.C., Hronsky, J.M.A., 2014. The Mineral System Concept: The Key to Exploration Targeting. Build. Explor. Capab. 21st Century.

Monteiro Santos, F.A., Mateus, A., Almeida, E.P., Pous, J., Mendes-Victor, L.A., 2002. Are some of the deep crustal conductive features found in SW Iberia caused by graphite? Earth Planet. Sci. Lett. 201, 353–367. https://doi.org/10.1016/S0012-821X(02)00721-5.

Moore, L.R., Bodnar, R.J., 2019. A pedagogical approach to estimating the co2 budget of magmas. Q. J. Geol. Soc. Lond. 176, 398–407. https://doi.org/10.1144/jgs2018-094.

Nelson, P.H., Van Voorhis, G.D., 1983. Estimation of sulfide content from induced polarization data. Geophysics 48, 62–75. https://doi.org/10.1190/1.1441408.

Newton, R.C., Tsunogae, T., 2014. Incipient charnockite: characterization at the type localities. Precambrian Res. 253, 38–49. https://doi.org/10.1016/j.precamres.2014.06.021.

Okudaira, T., Shigematsu, N., Harigane, Y., Yoshida, K., 2017. Grain size reduction due to fracturing and subsequent grain-size-sensitive creep in a lower crustal shear zone in the presence of a CO2-bearing fluid. J. Struct. Geol. 95, 171–187. https://doi.org/10.1016/j.jsg.2016.11.001.

Pirajno, F., 2021. Mineral systems and their putative link with mantle plumes. Geol. Soc. (Lond.) Spec. Publ. https://doi.org/10.1144/sp518-2020-276. SP518–2020–276.

Pommier, A., Kohlstedt, D.L., Hansen, L.N., Mackwell, S., Tasaka, M., Heidelbach, F., Leinenweber, K., 2018. Transport properties of olivine grain boundaries from electrical conductivity experiments. Contrib. Mineral. Petrol. 173, 1–13. https://doi.org/10.1007/s00410-018-1468-z.

Roberts, J.J., Duba, A.G., Mathez, E.A., Shankland, T.J., Kinzler, R., 1999. Carbon-enhanced electrical conductivity during fracture of rocks. J. Geophys. Res., Solid Earth 104, 737–747. https://doi.org/10.1029/1998JB900032.

Rumble, D., 2014. Hydrothermal graphitic carbon. Elements 10, 427–433. https://doi.org/10.2113/gselements.10.6.427.

Schlegel, T.U., Wagner, T., Fusswinkel, T., 2020. Fluorite as indicator mineral in iron oxide-copper-gold systems: explaining the IOCG deposit diversity. Chem. Geol. 548, 119674. https://doi.org/10.1016/j.chemgeo.2020.119674.

Schmeling, H., 2010. Dynamic models of continental rifting with melt generation. Tectonophysics 480, 33–47. https://doi.org/10.1016/j.tecto.2009.09.005.

Schmeling, H., 1986. Numerical models on the influence of partial melt on elastic, anelastic and electrical properties of rocks. Part II: electrical conductivity. Phys. Earth Planet. Inter. 43, 123–136. https://doi.org/10.1016/0031-9201(86)90080-4.

Schutt, D.L., Lowry, A.R., Buehler, J.S., 2018. Moho temperature and mobility of lower crust in the western United States. Geology 46, 219–222. https://doi.org/10.1130/G39507.1.

Selverstone, J., 2005. Preferential embrittlement of graphitic schists during extensional unroofing in the Alps: the effect of fluid composition on rheology in low-permeability rocks. J. Metamorph. Geol. 23, 461–470. https://doi.org/10.1111/j.1525-1314.2005.00583.x.

Selway, K., 2014. On the causes of electrical conductivity anomalies in tectonically stable lithosphere. Surv. Geophys. 35, 219–257. https://doi.org/10.1007/s10712-013-9235-1.

Shankland, T.J., Duba, A.G., Mathez, E.A., Peach, C.L., 1997. Increase of electrical conductivity with pressure as an indicator of conduction through a solid phase in midcrustal rocks. J. Geophys. Res., Solid Earth 102, 14741–14750. https://doi.org/10.1029/96jb03389.

Skirrow, R.G., van der Wielen, S.E., Champion, D.C., Czarnota, K., Thiel, S., 2018. Lithospheric architecture and mantle metasomatism linked to iron oxide Cu-Au ore formation: multidisciplinary evidence from the Olympic Dam Region, South Australia. Geochem. Geophys. Geosyst. 19, 2673–2705. https://doi.org/10.1029/2018GC007561.

Tamburello, G., Pondrelli, S., Chiodini, G., Rouwet, D., 2018. Global-scale control of extensional tectonics on CO 2 earth degassing. Nat. Commun. 9. https://doi.org/10.1038/s41467-018-07087-z.

Touret, J.L.R., Huizenga, J.M., Kehelpannala, K.V.W., Piccoli, F., 2019. Vein-type graphite deposits in Sri Lanka: the ultimate fate of granulite fluids. Chem. Geol. 508, 167–181. https://doi.org/10.1016/j.chemgeo.2018.03.001.

Vukmanovic, Z., Fiorentini, M.L., Reddy, S.M., Godel, B., 2019. Microstructural constraints on magma emplacement and sulfide transport mechanisms. Lithosphere 11, 73–90. https://doi.org/10.1130/L743.1.

Wang, D., Karato, S., Jiang, Z., 2013. An experimental study of the influence of graphite on the electrical conductivity of olivine aggregates. Geophys. Res. Lett. 40, 2028–2032. https://doi.org/10.1002/grl.50471.

Wang, L., Duan, J., Simpson, J., 2018. Electrical conductivity structures from magnetotelluric data in Cloncurry region. Rec. 2018/05. https://doi.org/10.11636/Record.2018.005.

Wannamaker, P.E., Doerner, W.M., 2002. Crustal structure of the Ruby Mountains and southern Carlin Trend region, Nevada, from magnetotelluric data. Ore Geol. Rev. 21, 185–210. https://doi.org/10.1016/S0169-1368(02)00089-6.

Waters-Tormey, C., Tikoff, B., 2007. Characteristics of a kilometer-scale high strain zone in the lower continental crust: Mt. Hay block, central Australia. J. Struct. Geol. 29, 562–582. https://doi.org/10.1016/j.jsg.2006.10.011.

Watts, K.E., Mercer, C.N., 2020. Zircon-hosted melt inclusion record of silicic magmatism in the Mesoproterozoic St. Francois Mountains terrane, Missouri: origin of the Pea Ridge iron oxide-apatite-rare earth element deposit and implications for regional crustal pathways of mineralizatio. Geochim. Cosmochim. Acta 272, 54–77. https://doi.org/10.1016/j.gca.2019.12.032.

Wickramasinghe, P.M., Palandagama, P.G.K.D., Dharmagunawardhane, H.A., 2018. A combined electromagnetic and resistivity survey for exploration for vein graphite: a case study over a Potential Graphite Field in the Sabargamuwa Province, Sri Lanka. J. Geol. Soc. Sri Lanka 19, 47. https://doi.org/10.4038/jgssl.v19i2.43.

Yang, X., Keppler, H., McCammon, C., Ni, H., 2012. Electrical conductivity of orthopyroxene and plagioclase in the lower crust. Contrib. Mineral. Petrol. 163, 33–48. https://doi.org/10.1007/s00410-011-0657-9.

Yardley, B.W.D., Bodnar, R.J., 2014. Fluids in the continental crust. Geochem. Perspect. 3, I–127. https://doi.org/10.7185/geochempersp.3.1.

Yardley, B.W.D., Valley, J.W., 1997. The petrologic case for a dry lower crust. J. Geophys. Res., Solid Earth 102, 12173–12185. https://doi.org/10.1029/97jb00508.

Yoshino, T., Noritake, F., 2011. Unstable graphite films on grain boundaries in crustal rocks. Earth Planet. Sci. Lett. 306, 186–192. https://doi.org/10.1016/j.epsl.2011.04.003.

Zhang, B., Yoshino, T., 2017. Effect of graphite on the electrical conductivity of the lithospheric mantle. Geochem. Geophys. Geosyst. 18, 23–40. https://doi.org/10.1002/2016GC006530.

Zhang, C., Duan, Z., 2010. GFluid: an Excel spreadsheet for investigating C-O-H fluid composition under high temperatures and pressures. Comput. Geosci. 36, 569–572. https://doi.org/10.1016/j.cageo.2009.05.008.